Journal of Bone and Mineral Research, 2025, **40**, 639–655
https://doi.org/10.1093/jbmr/zjaf040
Advance access publication: March 12, 2025
Research Article

Heme metabolism mediates RANKL-induced osteoclastogenesis via mitochondrial oxidative phosphorylation

Heng Qiu[1,2], Haiming Jin[1,3], Jiansen Miao[3], Hui Li[4], Junchun Chen[4], Xiaohong Yang[5], Xiaojun Chen[6], Benjamin H. Mullin[7,8], Kai Chen[1,6], Ronghe Gu[9], An Qin[1,10], Scott G. Wilson[1,7,11], Jiake Xu[1,4,*]

[1]School of Biomedical Sciences, University of Western Australia, Crawley, WA, 6009, Australia
[2]Department of Chemistry, The University of Hong Kong, Hong Kong SAR, 999077, China
[3]Department of Orthopaedic Surgery, The Second Affiliated Hospital and Yuying Children's Hospital of Wenzhou Medical University, Wenzhou, 325027, China
[4]Shenzhen University of Advanced Technology, and Shenzhen Institutes of Advanced Technology, Chinese Academy of Sciences, Shenzhen, 518055, China
[5]Guangzhou Institute of Traumatic Surgery, Guangzhou Red Cross Hospital of Jinan University, Guangzhou, 510220, China
[6]School of Molecular Sciences, The University of Western Australia, Crawley, WA, 6009, Australia
[7]Department of Endocrinology & Diabetes, Sir Charles Gairdner Hospital, Nedlands, WA, 6009, Australia
[8]Department of Endocrinology & Diabetes, Medical School, The University of Western Australia, Crawley, WA, 6009, Australia
[9]Department of Orthopedics, First People's Hospital of Nanning, Fifth Affiliated Hospital of Guangxi Medical University, Nanning, 530022, China
[10]Shanghai Key Laboratory of Orthopaedic Implant, Ninth People's Hospital, Shanghai Jiao Tong University School of Medicine, Shanghai, 200011, China
[11]Department of Twin Research and Genetic Epidemiology, King's College London, London, WC2R 2LS, United Kingdom

*Corresponding author: Jiake Xu, School of Biomedical Sciences, University of Western Australia, Crawley, WA, 6009, Australia, and Shenzhen University of Advanced Technology, and Shenzhen Institutes of Advanced Technology, Chinese Academy of Sciences, Shenzhen, 518055, China (jiake.xu@siat.ac.cn; jiake.xu@uwa.edu.au)

Abstract

Bone undergoes life-long remodeling, in which disorders of bone remodeling could occur in many pathological conditions including osteoporosis. Understanding the cellular metabolism of osteoclasts (OCs) is key to developing new treatments for osteoporosis, a disease that affects over 200 million women worldwide per annum. We found that human OC differentiation from peripheral blood mononuclear cells derived from 8 female patients is featured with a distinct gene expression profile of mitochondrial biogenesis. Elevated mitochondrial membrane potential (MMP, $\Delta\psi$m) was also observed in receptor activator of NF-κB ligand (RANKL)-induced OCs. Interestingly, the gene pathways of heme synthesis and metabolism were activated upon RANKL stimulation, featured by transcriptomic profiling in murine cells at a single-cell resolution, which revealed a stepwise expression pattern of heme-related genes. The real-world human data also divulges potential links between heme-related genes and bone mineral density. Heme is known to have a role in the formation of functional mitochondrial complexes that regulate MMP. Disruption of heme biosynthesis via genetically silencing Ferrochelatase or a selective inhibitor, N-methyl Protoporphyrin IX (NMPP), demonstrated potent inhibition of OC differentiation, with a dose-dependent effect observed in NMPP treatment and a substantial efficacy even at a single dose. In vivo study further showed the protective effect of NMPP on ovariectomy-induced bone loss in female mice. Collectively, we found that RANKL-mediated signaling regulated mitochondrial formation and heme metabolism to synergistically support osteoclastogenesis. Inhibition of heme synthesis impaired OC formation and reversed excessive bone loss, representing a new therapeutic target for metabolic skeletal disorders.

Keywords: osteoporosis, osteoclasts, heme, mitochondria, RANKL

Lay Summary

Bone remodeling is a lifelong process that can be disrupted in conditions like osteoporosis, a disease affecting over 200 million women globally per annum. Developing new treatments for osteoporosis requires understanding the cellular metabolism of osteoclasts (OCs), cells responsible for breaking down bone. In this study, we discovered that OC differentiation is characterized by increased mitochondrial biogenesis and elevated mitochondrial membrane potential (MMP). We also revealed that pathways involved in heme synthesis and metabolism were activated during this process, with real-world human data showing potential links between heme-related genes and bone mineral density. Heme is essential for forming functional mitochondrial complexes that regulate MMP and energy production, in which genetically knocking down heme catalyzing enzyme Ferrochelatase potently hampered receptor activator of NF-κB ligand (RANKL)-induced osteoclastogenesis. We found that a selective inhibitor of heme biosynthesis, N-methyl Protoporphyrin IX, effectively inhibited OC differentiation in a dose-dependent manner and protected against bone loss in estrogen-deficiency mice. These findings suggest that RANKL-mediated signaling regulates mitochondrial formation and heme metabolism to support osteoclastogenesis. Inhibiting heme synthesis could be a novel therapeutic target for treating metabolic skeletal disorders like osteoporosis.

Received: May 25, 2024. **Revised:** March 2, 2025. **Accepted:** March 6, 2025

Graphical Abstract

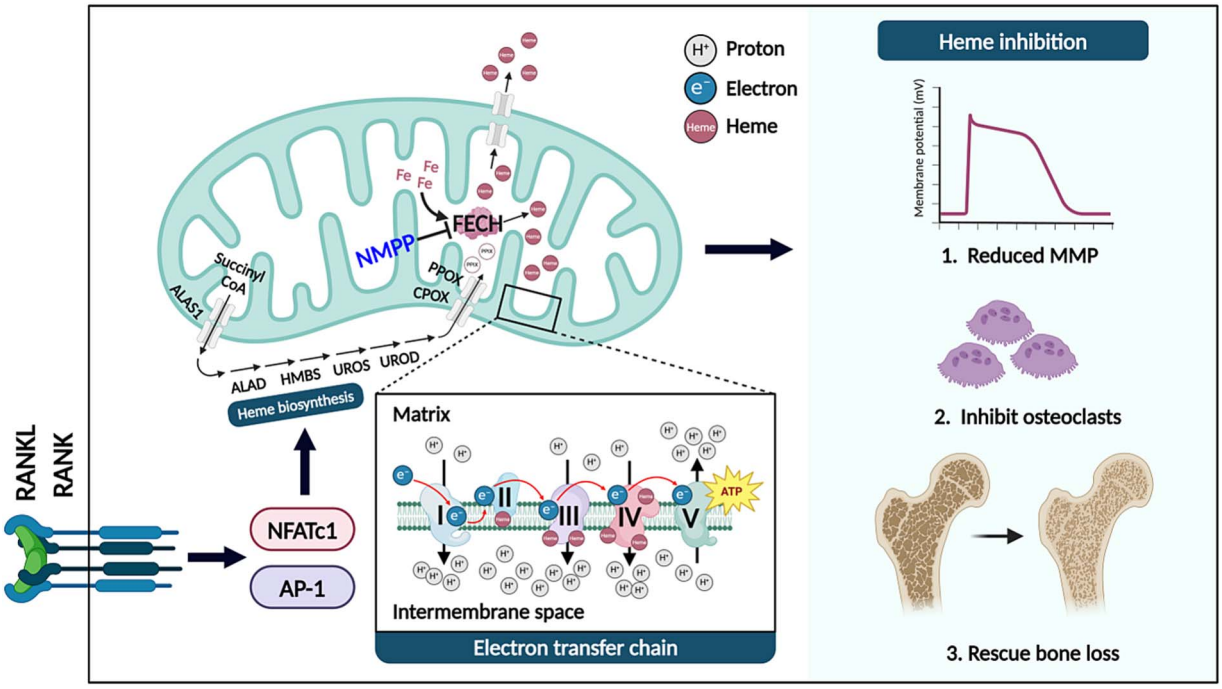

Introduction

Osteoporosis is a metabolic disease with signatures of excessive bone loss and deteriorated microarchitecture, causing millions of fractures per annum.[1] Pharmacological interventions include anticatabolic drugs, such as bisphosphonates and Denosumab, and anabolic drugs, eg, parathyroid hormone receptor agonists and Romosozumab. Nevertheless, medications alone can only prevent 20%-40% and 43%-53% of nonvertebral fractures, respectively, and a single use of any given osteoporosis treatment raises concerns like osteonecrosis of the jaw, atypical femoral fractures and limited sustainable curative effect.[2] Therefore, a better understanding of osteoclast (OC) metabolism may shed light on novel therapeutic targets.

Fusion of OCs and bone-resorbing activity are energy-demanding metabolic processes.[3–5] However, how receptor activators of NF-κB ligand (RANKL)-induced signals coordinate with mitochondria to fuel osteoclastogenesis and direct their cellular metabolism remains unclear. Here, we identified a stepwise expression pattern of gene set involved in heme metabolism during OC differentiation, coupled with elevated mitochondrial markers and an increased mitochondrial membrane potential (MMP, $\Delta\psi_m$). We are the first to report evidence hinting that heme metabolism is involved in osteoclastogenesis through participating in mitochondrial function and ATP production.

Materials and methods

Reagents

RAW264.7 cells were from ATCC. α-MEM, L-glutamine, and Penicillin-Streptomycin were produced by Harry Perkins Institute. Products from Thermo Fisher included FBS (16000044), Human RANKL protein (PHP0034), Glutaraldehyde solution, Lipofectamine3000, and JC-1 Dye (T3168). MTS Kit (G3580) was from Promega. TMRE Assay Kit (ab113852), c-FOS antibody (ab222699), Goat Anti-Rabbit IgG H&L (HRP) (ab205718), and Goat Anti-Mouse IgG H&L (HRP) (ab205719) were from Abcam. N-methyl Protoporphyrin IX (NMPP) (20846) came from Cayman Chemical. Santa Cruz Biotech supplied NFATc1 (sc-7294) and Ctsk (sc-48353) antibodies. Proteintech provided the Fech antibody (14466-1-AP). Western Lightning Ultra (NEL112001EA) was from PerkinElmer. All other chemicals were from Merck or as specified.

Subject recruitment and blood donation

Eight female patients aged 30-70 were recruited as indicated previously.[6] All subjects had self-reported European ancestry and confirmed that they were not experiencing medical conditions or using medications that would affect OC differentiation and bone resorption. All participants gave written informed consent and each patient donated 4 × 4 mL blood designated for this research. This study was approved by Sir Charles Gairdner and Osborne Park Health Care Group Human Research Ethics Committee (Approval Number: RGS0000001802).

Isolation of human peripheral blood mononuclear cells and in vitro osteoclastogenesis

Peripheral blood mononuclear cells (PBMCs) were isolated from 4 mL lithium heparin blood tubes using density gradient centrifugation. Tubes were centrifuged, buffy coats collected, diluted in PBS, and layered over Ficoll-Paque Premium. After further centrifugation and washing, PBMCs were suspended in complete α-MEM containing macrophage colony-stimulating factor (MCSF) (25 ng/mL). Two days later, the medium was changed to a medium containing MCSF and 100 ng/mL RANKL. The medium was replaced every

2-3 days for 12 days until OC-like cells formed. Cells were fixed with 4% PFA and stained with TRAcP.

RNA extraction, sequencing, and normalization

Total RNA was extracted from PBMCs and OCs using the RNA Mini Kit (QIAGEN). RNA samples were treated with DNase I to remove residual genomic DNA contamination. The integrity of the RNA was assessed using the Agilent 2100 Bioanalyzer, and only samples with RNA Integrity Numbers (RINs) ≥ 8.1 were used for sequencing. Gene expression quantitation was conducted by the Australian Genome Research Facility (AGRF) using 100 bp single-end RNA sequencing on the Illumina NovaSeq platform. Libraries were prepared using the TruSeq Stranded mRNA Library Prep Kit (Illumina). Raw sequencing reads were initially assessed using FastQC. Low-quality bases and adapter sequences were trimmed using Trimmomatic. Cleaned reads were aligned to the human genome reference (GRCh38/hg38) using STAR aligner (v2.7.0f) with default settings. Alignments were further checked for quality metrics. Gene-level counts were summarized using featureCounts (Subread v2.0), counting uniquely mapped reads per gene based on the GENCODE v38 annotation. Raw count data were transformed into Counts Per Million. Data normalization was performed using the Trimmed Mean of M-values with edgeR. Further normalization and differential expression analysis were performed using DESeq2 (v1.30.1), adjusting for batch effects and using an adjusted p-value threshold of $<.05$ for significance. Normalized data were exported into a GCT file format compatible with Gene Set Enrichment Analysis (GSEA).

Gene-based association testing

To determine whether there is evidence of an association between common variation in the human homologs of our genes of interest and bone density traits, we accessed publicly available summary genome-wide association study (GWAS) results for the largest GWAS performed to date for a bone structural trait—estimated BMD (eBMD).[7] Gene-based association testing on the GWAS summary results was performed using the VErsatile Gene-based Association Study 2 (VEGAS2) software.[8] This package maps variants to each gene region (±50 kb) and accounts for the linkage disequilibrium within each region while generating gene-based empirical association p-values. Correction for multiple testing was performed using the Bonferroni method as reported.[9,10]

scRNA-seq, bulk RNA-seq, and proteomic data processing

Public raw data (GSE147174) from the Gene Expression Omnibus was processed using the singleCellTK R package, including empty droplet detection, QC metrics, doublet prediction, and ambient RNA estimation. Downstream analysis with Seurat identified the top 2000 highly variable genes for principal component analysis, UMAP projection, and clustering. Cell markers from the original paper were used to identify osteoclastogenesis stages, and differentially expressed genes were determined using a Wilcoxon rank-sum test, where 1426 monocytic precursors, 200 OC progenitors, 3553 preosteoclasts, and 414 mature OCs were included.[11] Bulk RNA-seq data was obtained from the preprocessed gene list derived from the original paper,[11] and proteomic data from Andrew YH Ng's study (PXD009610).[12]

Protein structure visualization and interaction prediction

The structure of human Fech-PPIX bound complex was retrieved from Protein Data Bank (PDB: 3HCO) and visualized by PyMOL (Version 3.1.0). The close contacts and polar bonds between interactive residues of Fech and PPIX were determined by selecting all atoms within 4.0 of PPIX. The bindings of human/mouse Fech protein with NMPP or Griseofulvin were predicted *in silico* by Chai-1. The predicted complexes and interactive molecules were revealed by PyMOL.

Isolation of murine bone marrow macrophages and in vitro OC differentiation assay

Standard procedures for the isolation of bone marrow macrophages (BMMs) were well-established in our lab.[13,14] In general, fresh bone marrow cells were flushed out from long bones collected from C57BL/6J mice and maintained in MCSF (25 ng/mL)-containing medium for 6 h. Nonadherent cells were then transferred to new flasks and cultured in an MCSF-containing medium for another 3 days. To induce osteoclastogenesis, the medium was changed to a medium containing MCSF and 100 ng/mL RANKL on the day after seeding and replaced every 2 days until OCs formed. For TRAcP staining, cells were fixed with 4% PFA and stained with TRAcP solution for 2 h.

Cell proliferation assay (MTS assay)

RAW264.7 cells and fresh-isolated BMMs were seeded and treated with various concentrations of NMPP for 48 h. Cell culture media were then supplemented with media containing CellTiter 96 AQ_{ueous} One Solution Reagent. After incubation for 1-4 h, the absorbance of each well was measured by a BMG LABTECH microplate reader.

Measurement of heme concentration

The concentration of intracellular heme was determined as reported in the previous study.[15] Fresh-isolated BMMs treated with 100 ng/mL of RANKL with or without 5 μM NMPP were harvested and suspended in 2 M oxalic acid. The mixture was then heated at 100 °C for 30 min. The resulting protoporphyrin was quantified through fluorescence measurements. To ensure accurate results, the data were normalized to the endogenous protoporphyrin content and the overall protein concentration determined by BCA assay.

F-actin staining

BMMs were placed on coverslips in 24-well plates and treated with RANKL and NMPP until mature OCs formed in the positive control. Cells were fixed with 4% paraformaldehyde, blocked with phosphate-buffered saline (PBS) containing 3% bovine serum albumin (BSA), and incubated with rhodamine-phalloidin (1:300). After thorough washing, cells were stained with 4′,6-diamidino-2-phenylindole (DAPI) at 1:10 000 and visualized by NIKON A1Si Confocal Microscope.

Luciferase assay

RAW264.7 cells stably transfected with AP-1 or NF-κB luciferase reporter constructs were seeded into individual

wells of a 48-well plate and incubated overnight.[16] Subsequently, the cells were treated with 100 ng/mL RANKL and varying concentrations of NMPP for 48 h. The expression of luciferase was then quantified using the Promega Luciferase Assay System.

MMP ($\Delta\psi$m) detection

Upon formation of OCs, cells were stained with JC-1 and cultured at 37 °C for 10 min. After washing, cells were visualized under a confocal laser scanning microscope (Zeiss LSM 510 META system) at either Ex/Em 514/529 nm or Ex/Em 585/590 nm. TMRE (Tetramethylrhodamine, ethyl ester) was used to label active mitochondria and measure membrane potential. Fluorescence intensity was quantified using a microplate reader at Ex/Em 488/575 nm.

shRNA-mediated genetical modification

Knockdown shRNAs were designed and synthesized by Hunan Fenghui Biotechnology Co., Ltd. shRNA control (PLVX-shRNA2-puro) or shRNA targeting Fech gene was introduced into the freshly isolated BMMs through Lipofectamine3000 transfection reagent. The sequences of the shRNAs were as stated below: [GACGCTCTACGAACTGGATAT]. Twenty-four hours post-transfection, genetically manipulated BMMs were stimulated with 100 ng/ml RANKL for 5 days. Cells were then stained with TRAcP or collected for PCR and western blotting to quantitatively analyze the changes at mRNA and protein levels.

Real-time PCR

Total RNA was extracted by FastPure RNA Isolation Kit. Reverse transcription was performed and measured by HiScript II Q Select RT SuperMix (Vazyme Biotech) and ProFlex 3 × 32-well (Life Technologies). The real-time quantitative PCR was performed by QuantStudio 3 (Thermo Fisher). The thermal cycling conditions were set at 50 °C (2 min) and 95 °C (10 s), followed by 40 cycles of 95 °C (10 s), 60 °C (14 s), and a final elongation step at 95 °C (15 s), 60 °C (1 min). Primer sequences are listed in Table S1. The Ct values of the genes of interest were adjusted to Gapdh's Ct value. The data from the experimental groups were then further adjusted to the control groups to derive the ΔΔCt value.

Western blotting

Fresh BMMs with or without shRNA treatments were stimulated with 100 ng/mL RANKL for 5 days. Cells were lysed in RIPA buffer, followed by boiling with 5× loading buffer for 10 min. Samples were then separated on 7.5% SDS-denatured acrylamide gels and transferred onto 0.45 μm polyvinylidene fluoride membranes. The membranes were subsequently blocked using 5% nonfat milk powder in Tris-buffered saline with Tween 20 (TBST) that contained 10 mM Tris, 150 mM NaCl, and 0.1% Tween-20. This was followed by incubation with primary antibodies that were diluted (1:500-1000) in TBST with 1% BSA. HRP-linked secondary antibodies were diluted (1:20 000) in 1% BSA in TBST. Protein visualization was achieved using iBright 750 (Invitrogen).

Ovariectomized mouse model

All in vivo animal procedures were conducted in compliance with the principles and guidelines set by the Institutional Animal Ethics Committee of Wenzhou Medical University. 12-week-old female C57BL/6J mice were obtained from the Animal Center of the Chinese Academy of Science (Shanghai, China). These mice were randomly allocated into 3 groups: sham ($n = 6$), ovariectomized (OVX) ($n = 6$), and OVX with NMPP treatment ($n = 6$). To induce osteoporotic phenotypes, experimental mice underwent bilateral ovariectomies, while sham surgeries were performed on the sham group. Subsequently, a treatment group received NMPP injections every 2 days for 6 weeks. Meanwhile, the sham and OVX groups were administered an equal volume of saline as a control.

Micro-CT scanning and analysis

The femurs collected from euthanized mice were fixed in 4% paraformaldehyde for 48 h. They were scanned by Skyscan micro-CT (Bruker, Belgium) with the following parameters: a 0.5 mm aluminum filter for beam-hardening, a 0.4° rotation step, a 9 μm pixel size, and a source current and voltage of 500 μA and 50 kV. For further analysis, a refined volume of 0.5 mm below the growth plate and 1 mm in height was chosen for analyses using DATAVIEWER, CTAn, and CTVox software programs.

Histological and histomorphometric analyses

The femurs of the mice were fixed in 4% paraformaldehyde for 48 h. The samples were then decalcified in 10% EDTA solution for 14 days at 37 °C. The decalcified samples were embedded in paraffin and sectioned into 5 μm slices. Sections were subsequently stained with hematoxylin and eosin (H&E), tartrate-resistant acid phosphatase (TRAcP) or Runx2 and scanned by the uScope MXII Digital Microscope Slide Scanner. A region of interest located 0.5 mm below the growth plate and spanning 1 mm in height was chosen for the subsequent analysis by QuPath (v0.4.4).

Other analytical software and statistical methods

R language (3.6.3) and RStudio (1.4.1103) were used for RNA-seq data normalization, analysis, and plotting. DESeq2 and GSEA_4.1.0 performed gene enrichment analysis. GeneMANIA and STRING (11.5) analyzed gene–gene and protein–protein interactions. BioGPS explored tissue-specific gene expression. Chai-1 (Chai Discovery) and PyMOL (Version 3.1.0) were applied to predict and visualize protein structure and interactions. Prism 9 (9.5.1) created graphs. Student's *t*-test and One-way ANOVA conducted statistical analysis.

Results

RANKL induced a distinctive gene expression pattern and elevated mitochondrial activity

Human monocytes isolated from peripheral blood were stimulated with 100 ng/mL human RANKL until OC-like cells were formed, followed by RNA sequencing (Figure 1A). TRAcP-positive cells exhibited elevated levels of OC markers (Figure 1B and Figure S1A). Total RNA sequencing showed that 1926 genes (15%) were significantly upregulated by RANKL treatment, while 1457 genes (12%) were negatively regulated during osteoclastogenesis (Figure S1B). We observed that the mitochondrial marker genes were significantly upregulated in the OC-like cells (Figure 1C). To further profile the metabolic shift during OC differentiation, we measured the MMP ($\Delta\psi$m) upon RANKL treatment in murine bone marrow-derived macrophages (BMMs).[17] Cells were stained

with JC-1, a fluorescent marker that stays monomeric and emits green fluorescence when the mitochondrial membrane is in low potential but forms J-aggregates and emits red fluorescence when the membrane potential is increased. As observed in Figure 1D left panel, cells were evenly distributed across the field at day 0, accompanied by an approximately equal amount of green and red fluorescence signal, indicating quiescent mitochondrial activity. After 5-day RANKL treatment, monocytes formed OC-like cells with a notable leap in red fluorescence signal (Figure 1D left panel), suggesting an increased level of ATP production. Consistently, the overall fluorescent signal in differentiated OCs was more intensive than undifferentiated monocytes, which indicates hyperactive mitochondrial function following RANKL treatment (Figure 1D right panel).

RANKL induced upregulation of genes in the heme metabolism pathway

To understand the distinct gene expression changes that occur during osteoclastogenesis, we performed GSEA analysis to characterize differences in the expression profiles of human OC-like cells and their PBMC precursors. Figure S1C shows top enrichment pathways over osteoclastogenesis, including androgen,[18] cholesterol,[19] mTOR signaling,[20] fatty acids,[21] and glycolysis,[22] which are highly relevant to OC differentiation, maturation, function, and survival. Interestingly, we found that RANKL induced the expression of genes in the heme metabolism gene set (Figure 1E). The enrichment was accompanied by an upregulation of essential enzymes that mediate heme biosynthesis, including aminolevulinate dehydratase (ALAD), uroporphyrinogen III synthase (UROS), uroporphyrinogen decarboxylase (UROD), coproporphyrinogen oxidase (CPOX), and ferrochelatase (FECH) and coupled with an elevated level of heme concentration (Figure 1F and G). Totally 183 genes related to the heme metabolism pathway were assessed, with 38% of them differentially expressed in the OC-like cells, indicating that heme activity is a potential signature of OC differentiation. Figure S2 presents a heatmap displaying the different heme metabolism gene expression patterns of PBMCs and OCs. The top 40 differentially regulated genes were presented in detail with fold changes and *p*-value, including genes like peroxiredoxin 2, which has been shown to be co-expressed with the core machinery of heme synthesis.[23] Heme-related genes highly expressed in differentiated OCs, like transferrin receptor 1 (TFRC) and carbonic anhydrase 2 (CA2), have been associated with OC function and bone volume.[24,25] Exploration of tissue-specific expression of heme-related genes suggested that E2F transcription factor 2 (E2f2), Fech, kell metallo-endopeptidase (Kel) and transmembrane and coiled-coil domain family 2 (Tmcc2) were highly and selectively expressed in murine bone marrow and bone tissue (Figure S3).[26] Moreover, the expression of sodium- and chloride-dependent creatine transporter 1 (Slc6a8), another heme metabolism-related gene enriched in RANKL-treated cells, was significantly elevated in OC differentiation and lipopolysaccharide-stimulated BMMs, whereas it was hardly detected in bone marrow or bone tissue, suggesting that OCs are the main source of Slc6a8 in the bone environment (Figure S4). These expression patterns imply the regulatory role of heme in skeletal homeostasis. In addition, by crosschecking with the ENCODE Transcription Factor Targets Dataset, we noticed that most of the highly upregulated genes in Figure S2 and heme synthesis-related enzymes are the targets of transcription factors NFATc1 and activator protein 1 (AP-1) (FOS/JUN) (Table S2).[23,27] The volcano plot (Figure S5A) specifically highlighted the most differentially regulated genes (Log fold-change $>=2$ and p-value $<.0001$) in heme metabolism during OC differentiation, accompanied with the protein–protein interaction network derived from STRING which further predicted the interactions between these genes at the protein level (Figure S5B). With the support of a very large size of functional association data (Genemania, indexing 2830 association networks containing 660 554 667 interactions mapped to 166 691 genes from 9 organisms), we were able to predict the connections in our Volcano plot-derived gene set from multiple perspectives. As shown in Figure S6, strong and complex co-expression and co-localization connections were seen in the differentially regulated genes selected from the Volcano plot. Genes such as Acyl-CoA synthetase long-chain family member 6 (ACSL6), oxysterol binding protein 2 (OSBP2), and RAP1 GTPase activating protein (RAP1GAP) were found to interact with multiple targets that are also tightly regulated during osteoclastogenesis, indicating that they may be hub genes which can be considered as therapeutic targets.

RANKL regulated heme metabolism, biosynthesis, and catabolic processes

Next, we examined the enriched genes by comparing them to the genes involved in heme metabolic processes according to the Gene Ontology Consortium (GO: 0006783). The dot bar graph in Figure 2A shows the mRNA level, based on our transcriptome analysis, of 32 heme-related genes annotated in GO:0006783. Many of these genes were differentially expressed during osteoclastogenesis and are known to regulate heme metabolic activity, heme biosynthesis, and heme catabolic process, eg, ATP-binding cassette super-family B member 6 (ABCB6) and heme-binding protein 1 for heme metabolism, protoporphyrinogen oxidase (PPOX), ALAD, UROD, UROS, hydroxymethylbilane synthase (HMBS), solute carrier family 22 member 4, iron-sulfur cluster assembly 1, solute carrier family 11 member 2 (SLC11A2), CPOX, and transmembrane protein 14C (TMEM14C) for heme biosynthesis, biliverdin reductase A and biliverdin reductase B for heme catabolic effect and heme oxygenase 2 (HMOX2) for heme oxidation.[28] We further explored how these genes are reciprocally connected. A network was constructed in Genemania, which exhibited strong physical interactions shared by these genes (Figure S7A). 5′-Aminolevulinate synthase 1 (ALAS1), ALAD, CPOX, FECH, HMBS, PPOX, UROD, UROS are 8 known enzymes required for heme synthesis. Consistently, it was revealed that these genes share stronger connections among them, both in gene and protein levels (Figure S7B).[23] Interestingly, genes like frataxin, heme oxygenase 1, HMOX2, SLC11A2 and sorting nexin 3 were not only regulated by RANKL but also well-connected among them in gene and protein networks, implicating their central roles on heme regulation. Through manipulating these genes, RANKL-RANK signaling is engaged to modulate heme function, potentially facilitating OC formation.

Human GWAS data suggested a potential link between heme biosynthesis genes and bone mineral density

To gain insights from genome-wide human data, we investigated each gene that encodes essential enzymes for heme

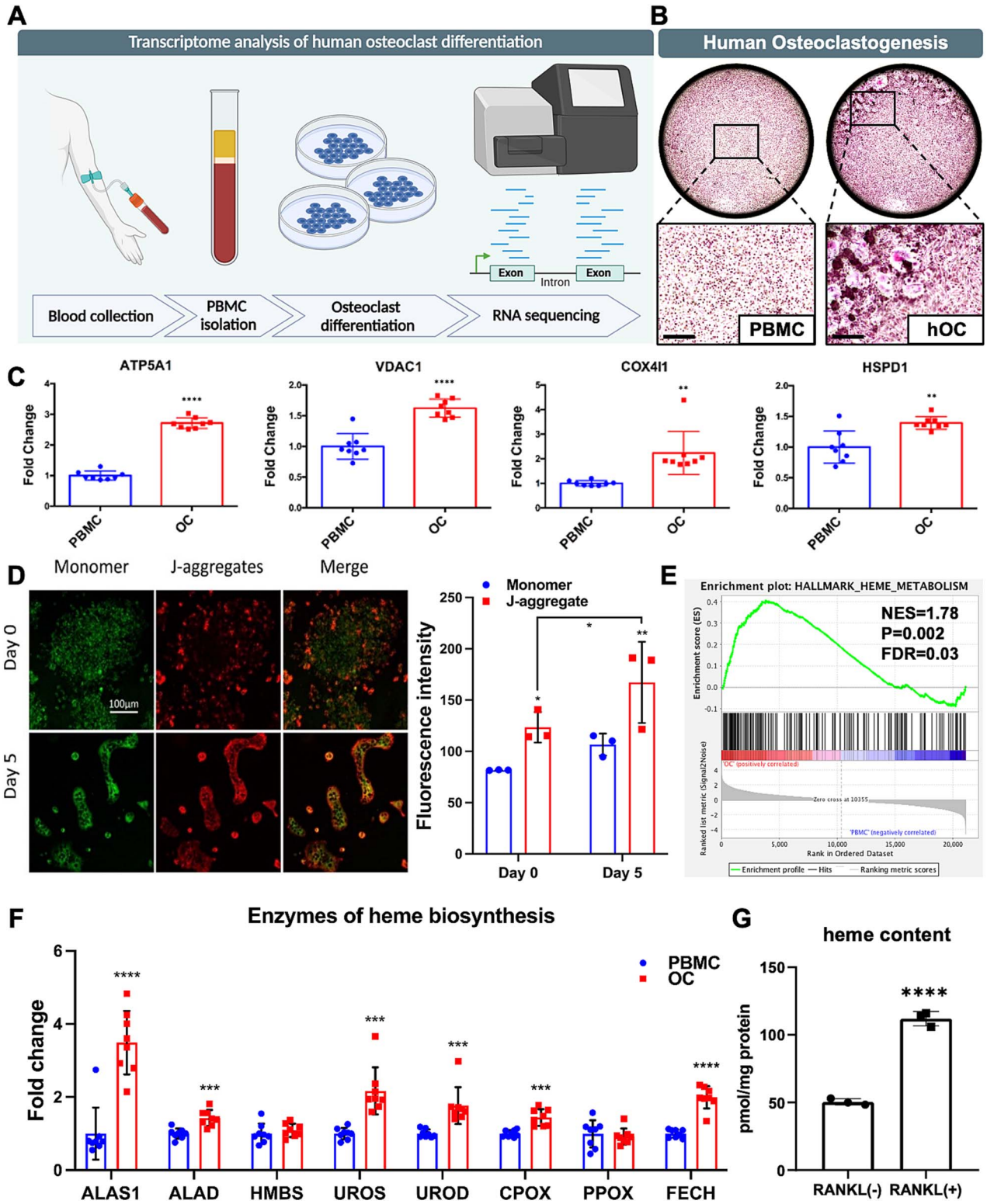

Figure 1. Transcriptome and GSEA analysis of gene expression in human OCs versus monocytes. (A) Brief illustration of transcriptome analysis of human OC differentiation. (B) TRAcP-positive human OCs with an enlarged image showing staining details. Scale bar = 200 μm. (C) The fold changes of mitochondrial markers during human OC differentiation. $n = 8$ pairs. (D) Fluorescence staining of JC-1 in RANKL-induced murine osteoclastogenesis. Increased J-aggregates suggests an elevated MMP ($\Delta\psi$) induced by RANKL. Result was quantified by comparison of the fluorescence intensity of J-aggregates and monomers before and after 5-day RANKL treatment. Scale bar = 100 μm. $n = 4$. (E) GSEA enrichment plot in heme metabolism (MSigDB gene set: HALLMARK_HEME_METABOLISM). (F) Gene expression levels of essential enzymes for heme biosynthesis. (G) Heme content in murine BMMs treated without/with RANKL ($n = 3$). All data are displayed as mean ± SD. *$p < .05$, **$p < .01$, ***$p < .001$, and ****$p < .0001$ compared to PBMC or indicated otherwise.

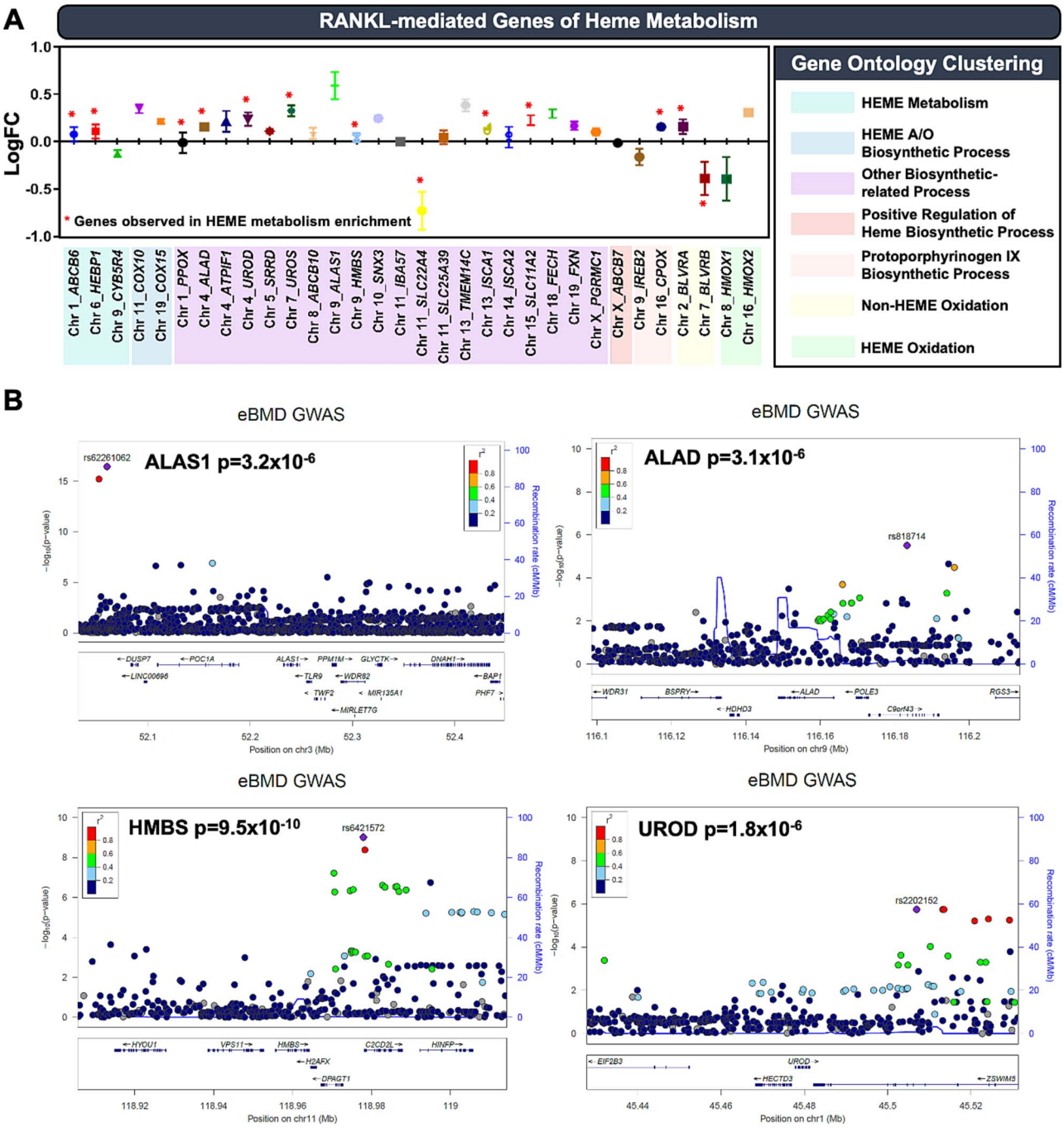

Figure 2. RANKL regulates different biological processes of heme metabolism that are potentially associated with estimated bone mineral density (eBMD) by human GWAS. (A) The dot bar chart specifies the genes that modulate the biological processes of heme metabolism and their corresponding fold changes derived from our RNA sequencing dataset. $n = 16/8$ pairs. The bar graph is displayed as mean ± SD. (B) Regional association plots depicting eBMD GWAS results for genes encoding essential enzymes of heme biosynthesis. Genetic variants within 200 kb of each gene are plotted according to their chromosomal location (*x*-axis) and eBMD *p*-value (−log10) (*y*-axis). Variants are color-coded according to the degree of linkage disequilibrium (1000GP Nov 2014 EUR population) with the lead variant at each locus, with the recombination rate indicated by the blue line.

biosynthesis (±50 kb) using data from the largest GWAS performed for a bone structural trait (eBMD).[9,10] A number of single nucleotide polymorphisms in the ALAS1, ALAD, HMBS and UROD gene regions demonstrated genome-wide suggestive ($p < 5 \times 10^{-6}$) or genome-wide significant ($p < 5 \times 10^{-8}$) associations with eBMD (Figure 2B and Table S3), most notably for HMBS (rs6421572, $p = 9.5 \times 10^{-10}$). However, it remains inconclusive whether these associations are specifically related to these genes. Other heme-related genes of interest, eg, FECH, CPOX, UROS, and PPOX, did not demonstrate significant associations with eBMD (Data not shown). This may be attributed to the intricate nature of the genetic methodology involved, which could obscure potential associations.

Dissecting RANKL-induced stepwise expression pattern of mitochondrial and heme-related genes at a single-cell resolution

We acquired single-cell RNA sequencing data (GEO: GSE147174) to examine whether an alike gene expression

pattern is observed in murine osteoclastogenesis and analyze the organization of temporal expression patterns at a single-cell resolution.[11] Cells were collected on day 0, day 1, and day 3 post-RANKL treatment for single-cell RNA sequencing (scRNA-seq). A total of 2190, 2649, and 2389 cells on day 0, day 1, and day 3, respectively, were profiled to generate the stepwise differentiation trajectory of OCs (Figure 3A). Mitochondrial markers, including Atp5a1, Vdac1, Cox4i1, and Hspd1, were upregulated during OC differentiation in a temporally organized and stepwise manner, consistent to our previous observation (Figure 3B and D). Following RANKL treatment, the expression of heme-related genes, Alas1, Alad, Hmbs, Uros, Urod, Cpox, Ppox, and Fech, was dynamically changed in sequence of OC differentiation and heme biosynthetic pathway (Figure 3C and D). Alas1 expression, which is the first and rate-limiting enzyme in the mammalian heme biosynthetic pathway, was elevated in the earliest stage of osteoclastogenesis, followed by significant increases in Alad and Hmbs, critical enzymes that carry the second and third-step reactions, respectively, in heme production. Both Alas1 and Alad genes were downregulated in mature OCs, indicating the completion of their duty, while Hmbs remained highly expressed. The expression levels of Uros, Urod, and Cpox reached a relatively high level in preosteoclasts and were maximized in mature OCs. Ppox and Fech, the enzymes responsible for the second-last and terminal steps, respectively, in heme biosynthesis, showed no considerable change in their transcriptomic expression in OC progenitors and preosteoclasts; however, their expression was significantly upregulated and reached the peak in mature OCs. Following the trajectory of OC differentiation, the upregulation of mitochondrial markers is highly coupled with a dynamic and sequential expression of heme biosynthesis genes. In parallel, we analyzed the time-course bulk-seq dataset from the same study (GEO: GSE147174), along with independent proteomic data (ProteomeXchange Dataset PXD009610-1) derived from Andrew YH Ng's study; nevertheless, the unique expression patterns of certain heme-related genes appeared to be obscured, likely due to the loss of information on the heterogeneity and diversity within distinct cell populations that is inherent to bulk sequencing methods (Figure S8).[11,12] Of note, the high expression level of FECH in RANKL-stimulated cells was consistent across scRNA-seq, bulk RNA-seq and proteomic analysis.

Knockdown of Fech gene disrupted RANKL-mediated osteoclastogenesis

Ferrochelatase, a highly upregulated gene by RANKL (Figure 1E), is an enzyme that controls the terminal step of heme biosynthesis. To further elucidate the biological effect of heme in RANKL-induced osteoclastogenesis, we knocked down the Fech gene in freshly isolated BMMs using shRNA and induced them with or without RANKL. As shown in Figure 4A, RANKL successfully induced the formation of mature OCs in BMMs treated with shRNA control (sh-NC), while RANKL did not induce TRAcP+ multinucleated OCs after treatment with shRNA targeting Fech. rtPCR quantitatively showed that RANKL-induced osteoclastic marker genes were significantly downregulated in Fech deficient BMMs upon 5-day RANKL stimulation, consistent to TRAcP staining result (Figure 4B). The phenotypic changes induced by Fech knockdown were also examined at protein level and an accordant result was achieved, which manifests the markedly reduced levels of osteoclastic proteins following Fech disruption (Figure 4C and D). Taken together, these data provided genetic evidence regarding the role of Fech in RANKL-mediated OC differentiation.

RANKL regulated OC differentiation through coupling heme with mitochondrial OXPHOS

Heme is involved in the formation of functional mitochondrial complexes II, III, and IV, which are the major components of the electron transport chain that fuels OC differentiation. Heme biosynthesis selective modulators, NMPP, and Griseofulvin, an FDA-approved antifungus drug, have been proposed to regulate mitochondrial function via inhibiting FECH[23,29–31] (Figure 5A). To elucidate the molecular basis of NMPP and Griseofulvin, we first studied the crystal structure of FECH and PPIX bound (PDB: 3HCO) which clearly shows the interactive residues and polar contacts formed with PPIX (Figure 5B). An artificial intelligence (AI)-driven multimodal foundation model (Chai Discovery) was then applied to model interactions between NMPP and FECH (Figure 5C and D). All interactive residues are shown in amino acids, where blue and red colors label shared contacts between PPIX-FECH and NMPP-FECH complexes. In particular, red color labeled residues are predicted to form polar contacts in the catalytic site. As shown, NMPP can competitively inhibit the formation of PPIX-FECH complex, reducing the synthesis of heme. Similarly, *in silico* modellings of Griseofulvin-FECH complex also indicate that Griseofulvin can compete the binding site in the catalytic core with PPIX (Figure 5E and F). All interactive residues, including those which form polar bonds, are highly conserved across a wide variety of species (Figure S9). Experimentally, to investigate whether disruption of heme metabolism impairs cell energy production and OC differentiation, we treated mouse cells with different doses of NMPP during osteoclastogenesis culture. A wide range of concentrations of NMPP showed no evident cytotoxicity in fresh-isolated BMMs or RAW264.7 cells (Figure S10A and B). RANKL-induced OC differentiation of BMMs was dose-dependently suppressed by NMPP treatment (1-10 μM) (Figure 6A and B). The inhibition of osteoclastogenesis by NMPP is coupled with a reduced level of heme concentration (Figure 6C). A similar effect was seen in OC culture from RAW264.7 cells (Figure S10C). Of note, suppression of Fech will potentially lead to the accumulation of PPIX, a precursor of heme. However, 5-40 μM of PPIX treatment did not present any effect on OC differentiation, indicating that NMPP-mediated inhibition of osteoclastogenesis was due to heme deficiency (Figure S10D). Forming a sealing zone is the prerequisite of efficient bone resorption, as it facilitates the secretion of proteolytic enzymes in a bone-anchored adhesion structure. As shown in Figure 6D, RANKL-induced multinucleated OCs encompassed by Rhodamine Phalloidin-labeled podosome belts. The formation of these delicate structures was completely abolished by 5 μM NMPP treatment, suggesting that NMPP effectively inhibited the differentiation of functional OCs. In vitro OC formation requires consecutive stimulation with RANKL on day 1, day 3, and day 5. Interestingly, we found that treating cells with 5 μM NMPP on day 3 only presented a stronger inhibitory effect on OC differentiation than those of day 1 and day 5 only (Figure 6E). This profound effect is possibly attributed to the mitochondrial biosynthesis,

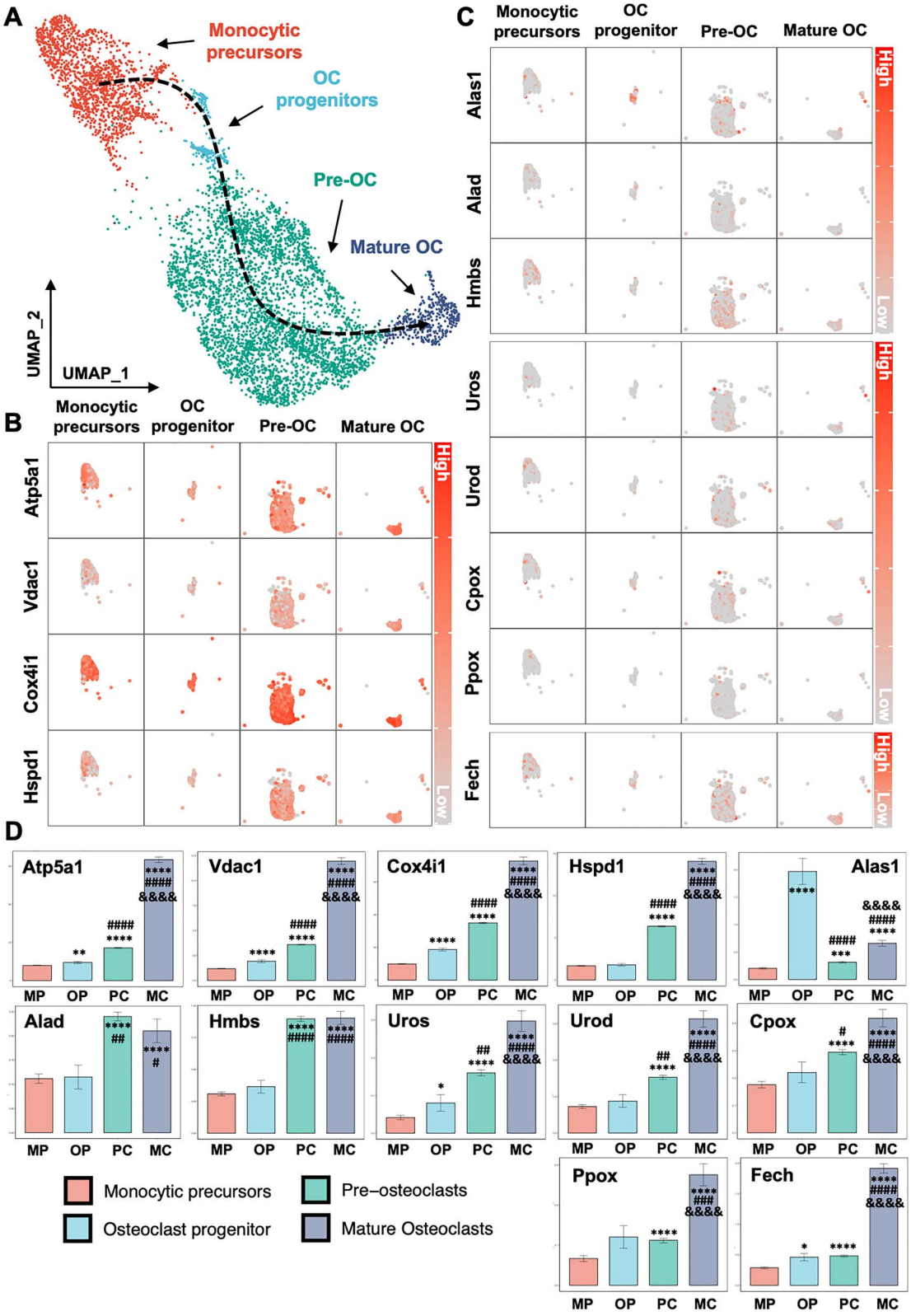

Figure 3. Deciphering RANKL-induced expression pattern of mitochondrial markers and heme-related genes in murine osteoclastogenesis at single-cell resolution. (A) The trajectory of OC differentiation was estimated by pseudotime analysis and mapped on a UMAP visualization. (B) Stepwise expression of mitochondrial markers during OC differentiation. (C) Dynamic and sequential expression of heme biosynthesis genes following the trajectory of osteoclastogenesis at single-cell resolution. (D) Quantification and statistical analysis of the expression pattern of mitochondrial markers and heme-related genes. All data are presented as mean ± SD. $^{*}p < .05$, $^{**}p < .01$, $^{***}p < .001$ and $^{****}p < .0001$ OP, OC and MC compared to MP; $^{\#}p < .05$, $^{\#\#}p < .01$, and $^{\#\#\#\#}p < .0001$ PC and MC compared to OP; $^{\&\&\&\&}p < .0001$ MC compared to PC.

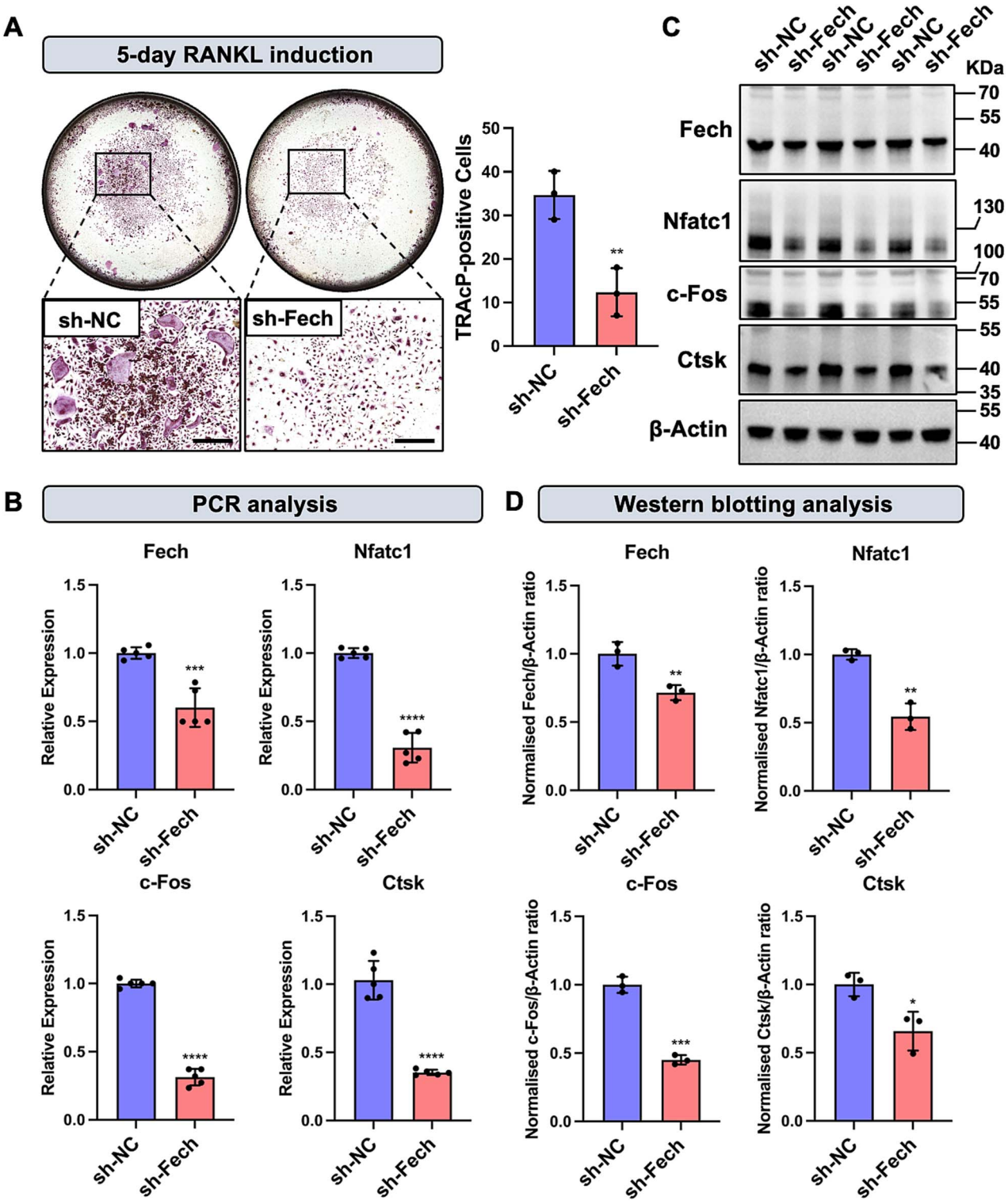

Figure 4. Knockdown of Fech gene disrupted OC differentiation. (A) Left panel: shRNA-mediated Fech knockdown significantly impaired RANKL-induced TRAcP-positive multinucleated cells from BMMs. Scale bar = 200 μm. Right panel: Statistical analysis of TRAcP staining. $N = 3$. All data are presented as mean ± SD. $^{**}p < .01$ compared to sh-NC group. (B) rtPCR revealed that osteoclastic genes were profoundly downregulated following Fech knockdown during RANKL-mediated differentiation. $n = 5$. All data are presented as mean ± SD. $^{***}p < .001$ and $^{****}p < .0001$ compared to sh-NC group. (C) A consistent result is supported by western blotting, which shows decreased protein levels of osteoclastic markers in *Fech deficient* BMMs upon RANKL stimulation. (D) Statistical analysis of western blotting results. Each protein expression was normalized to β-actin and quantified by ImageJ based on gray intensity. $N = 3$. All data are presented by the mean ± SD. $^{*}p < .05$, $^{**}p < .01$, and $^{***}p < .001$ compared to sh-NC.

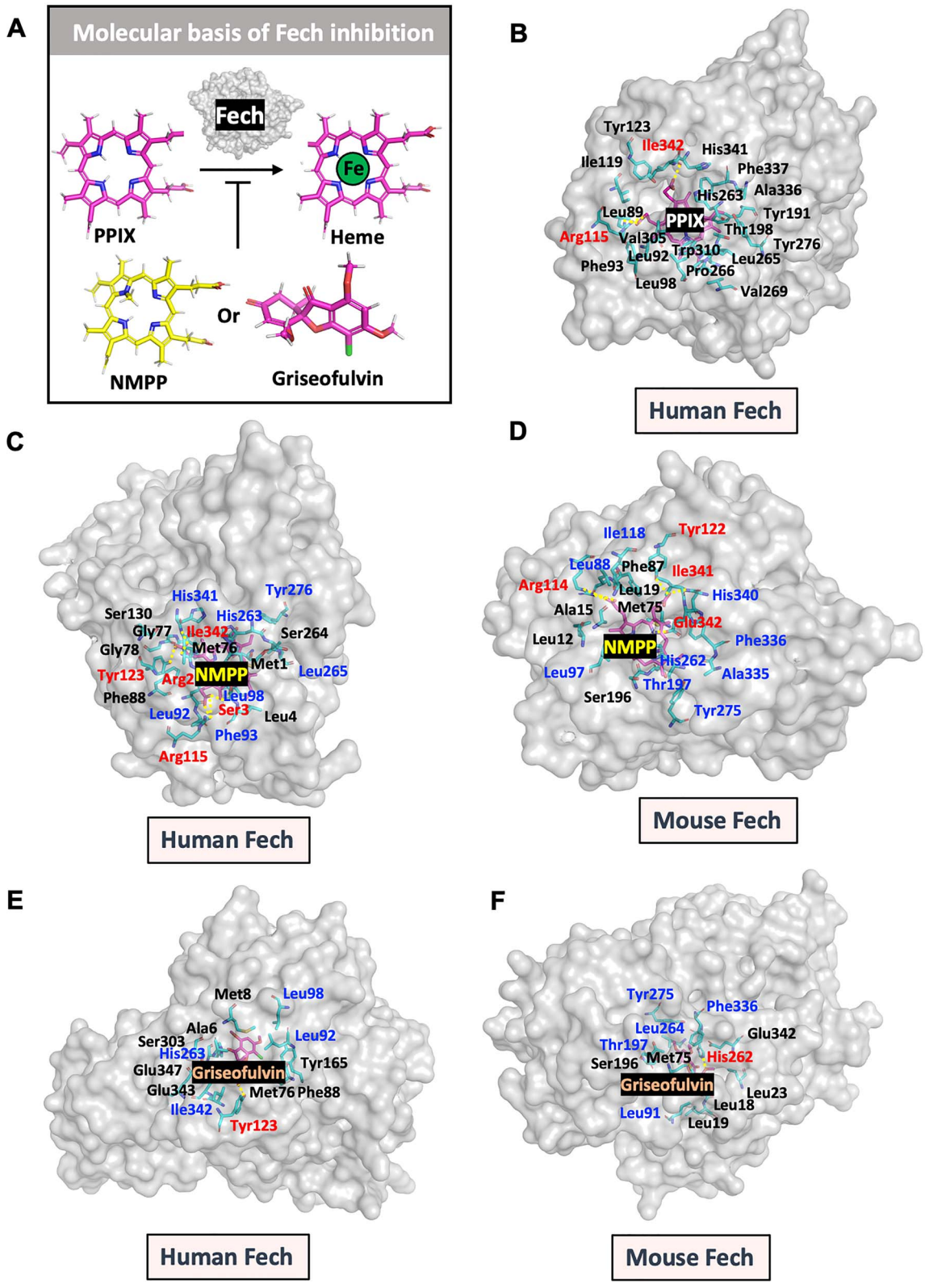

Figure 5. The molecular basis of heme biosynthesis inhibitors. (A) NMPP and Griseofulvin, an FDA-approved antifungus drug, were reported to inhibit heme biosynthesis via FECH, which catalyzes the terminal step in the biosynthesis of heme, converting protoporphyrin IX (PPIX) into heme B. (B) The crystal structure of FECH and PPIX bound (PDB: 3HCO) showing interactive residues and polar contacts (red color-labeled residues and yellow dash line) with PPIX. (C) and (D) Artificial intelligence model (chai discovery) was used to mimic NMPP-human/mouse FECH interactions. Red color highlights residues predicted to form polar contacts (yellow dash line) with NMPP and blue color labels interactive residues that also involve PPIX binding. (E) and (F) Chai discovery was used to predict Griseofulvin-human/mouse FECH interactions. Red color highlights residues potentially forming polar contacts (yellow dash line), and blue color highlights interactive residues that mediate PPIX binding.

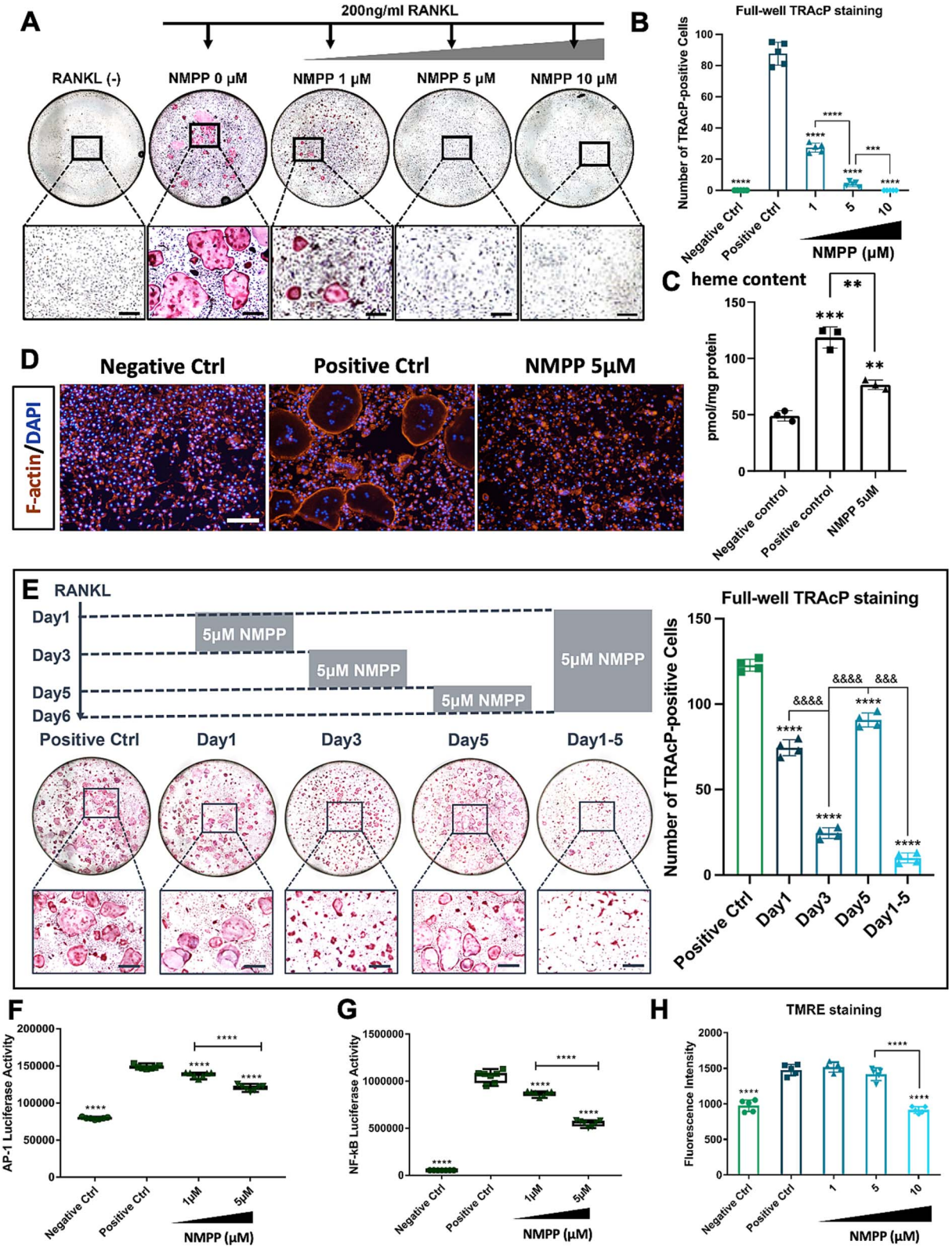

Figure 6. In vitro therapeutic potentials of heme biosynthesis inhibitor NMPP. (A) NMPP suppressed osteoclastogenesis in a dose-dependent manner. Representative images are presented with TRAcP staining. Scale bar = 200 μm. (B) TRAcP-positive multinucleated cells were quantified in a bar chart by ImageJ. $N = 5$. (C) Heme content in BMMs, BMMs stimulated with RANKL, and BMMs treated with both RANKL and 5 μM NMPP. $N = 3$. Data are presented as mean ± SD. $^{**}p < .01$ and $^{***}p < .001$ compared to negative control group or as indicated. (D) Podosome belt staining shows the dose-dependent inhibition of osteoclastogenesis induced by NMPP. Scale bar = 200 μm. (E) Time-course OC formation assay indicates that a single-dose treatment of NMPP at day 3 achieved a stronger inhibitory effect than those of day 1 and day 5 only. Left panel: Representative images of full-well TRAcP staining with enlarged regions of interest. Scale bar = 200 μm. Right panel: Quantification of full-well TRAcP-positive multinucleated cells. $N = 4$. All data are presented as mean ± SD. $^{****}p < .0001$ compared to positive ctrl. $^{\&\&\&}p < .001$ and $^{\&\&\&\&}p < .0001$ compared to day3. (F) and (G). Heme inhibition by NMPP suppressed the activity of transcriptional factors AP-1 and NF-κB in a dose-dependent manner. (H) The fluorescence intensity of TMRE staining reflected the MMP in live cells. $N = 5$. All data are presented as mean ± SD. $^{**}p < .01$, $^{***}p < .001$ and $^{****}p < .0001$ compared to positive ctrl group unless indicated otherwise.

in which the copy number of mitochondrial complexes is most upregulated in day 3, and the coupled expression pattern of Fech gene.[32] To understand the effect of heme inhibition on the underlying signaling transduction, we measured the activities of 2 transcription factors, AP-1 and NF-kB, through luciferase assay. Both transcription factors' activities were dose-dependently suppressed, accordant to the osteoclastogenesis assay and podosome-belt staining (Figure 6F and G). We further explored whether the inhibition of OC formation was due to the impaired MMP led by NMPP. Fresh BMMs were stimulated with RANKL in the presence or absence of NMPP for 5 days until OCs formed in the positive control group. Cells were then stained with TMRE to quantify changes in MMP based on the intensity of the fluorescence signal. The elevation of MMP during OC differentiation was sabotaged by NMPP treatment in a dose-dependent manner (Figure 6H). A consistent result was also observed in the OC culture of RAW264.7 cells (Figure S10E), consolidating our previous observations.

NMPP treatment alleviated OVX-induced bone loss

Our in vitro results have demonstrated that NMPP treatment possesses inhibitory properties on OC formation and function, in which a consistent result was observed with Fech knockdown. We further investigated the antiosteoporosis potential of NMPP as a chemical agent using an OVX-induced osteoporosis mouse model. Mice underwent either OVX or sham surgery, followed by intraperitoneal injections of 5 mg/kg NMPP or a vehicle-only solution every consecutive day for 6 weeks (Figure 7A). No adverse events, fatalities or notable changes in body weight occurred following the OVX procedure and NMPP administration. Micro-CT analysis of mice femurs showed that NMPP effectively prevented excessive bone loss caused by estrogen deficiency (Figure 7B), supported by the quantitative evaluations of bone parameters showing elevated bone volume (BV/TV) and trabecular number (Tb.N) and reduced trabecular separation (Tb.Sp) in NMPP-treated mice (Figure 7C). However, the thickness of trabeculae (Tb.Th) remained unchanged (Figure 7C). Histologically, quantifications of hematoxylin and eosin (H&E) staining revealed that bone surface was well-preserved in NMPP-treated group in comparison to nontreated group, consistent with the micro-CT results (Figure 7D upper panel and Figure 7E). The femur sections were also stained for TRAcP and Runx2 to visualize OCs and osteoblasts, respectively. As depicted in Figure 7D bottom panel and Figure 7E, OVX procedure resulted in increased surface area of TRAcP-positive OCs (Normalized to bone surface), which was evidently reversed by NMPP treatment. In contrast, Runx2 was not changed significantly (Figure S11). Collectively, we found that RANKL induced mitochondrial formation and heme biosynthesis in monocytes, synergistically boosting energy production to support OC differentiation. Disruption of heme metabolism by a heme inhibitor has a potential influence on bone density and strength (Figure 8).

Discussion

Our transcriptome and in vitro analysis identified significant increases in mitochondria markers and MMP, an indicator of OXPHOS, during RANKL-induced human OC differentiation. Osteoclastogenesis and bone resorption are intensive energy-consuming cellular metabolic processes.[3] Evidence shows that aerobic respiration is upregulated when monocytes are fusing into bone-resorbing OCs.[3–5] Larger mitochondria were also seen in mature OCs, along with elevated cristae and more sophisticated mitochondrial networks.[3] Our further analysis revealed a link between active mitochondrial biogenesis and the activation of heme metabolism-related genes, such as TFRC and CA2, which play crucial roles in bone remodeling.[24,25] This is further confirmed by in vitro osteoclastogenesis assays that show an increase in heme concentration following RANKL treatment. Tissue-specific expression of heme-related genes like Slc6a8, E2f2, Fech, Kel, and Tmcc2 in differentiated OCs, bone marrow, and bone tissue supports the potential regulatory role of heme in the bone environment.[33] Our bioinformatic analysis also identified hub genes (eg, ACSL6, OSBP2, and RAP1GAP) and their interactions with highly regulated heme genes during osteoclastogenesis. To examine the clinical significance of heme pathway in bone metabolism, we investigated associations between heme biosynthesis enzymes and estimated bone mineral density (eBMD) via GWAS data. Significant associations were seen in the ALAS1, ALAD, HMBS, and UROD gene regions, while their exact correlations have yet to be biologically determined. Considering the difference between human and murine, we analyzed single-cell RNA sequencing data to investigate the stepwise differentiation trajectory of murine OCs at a single-cell resolution.[11] Our analysis revealed a trend of increased mitochondrial activity, consistent to previous observations. Following RANKL treatment, we observed a dynamic expression of heme-related genes, such as Alas1, Alad, Hmbs, Uros, Urod, Cpox, Ppox, and Fech, in the sequence of OC differentiation and the heme biosynthetic pathway. Alas1 expression, the first and rate-limiting enzyme for heme synthesis, was elevated at the earliest stage of osteoclastogenesis, with subsequent increases in Alad and Hmbs, which catalyze the second and third-step reactions in heme production. Both Alas1 and Alad were gradually downregulated in mature OCs, indicative of a completion of their function, whereas the expression of Hmbs remained significantly high. The expression of other heme genes like Uros, Urod, and Cpox was gradually increased following the stepwise cell fate of OCs. Ppox and Fech, essential enzymes responsible for the second-last and terminal steps in heme biosynthesis, were only seen upregulated at maximum in mature OCs. The unique expression patterns of certain heme-related genes, eg, Hmbs and Ppox, could not be distinguished in our human OC bulk RNA-seq dataset or the murine OC bulk RNA-seq dataset, possibly due to limited test timepoints and the loss of information on the heterogeneity and diversity within cell populations. Of note, the expression level of FECH was consistently high in OCs both at gene and protein levels across all the datasets we analyzed.

In cells, heme is critical for aerobic respiration, as mitochondrial complexes II, III, and IV demand heme to serve as a prosthetic group, and the disruption of heme metabolism may lead to mitochondrial dysfunction.[34–36] Despite pivotal functions in life, heme is cytotoxic; therefore, its synthesis is strictly tuned. Heme metabolism is regulated by many factors, but we noticed that most upregulated heme-related genes in our dataset were controlled by NFATc1 and AP-1, which are the master transcription factors of OC differentiation. Given to the relationship between RANKL, heme, and mitochondria, we hypothesized that RANKL mediates heme metabolism and

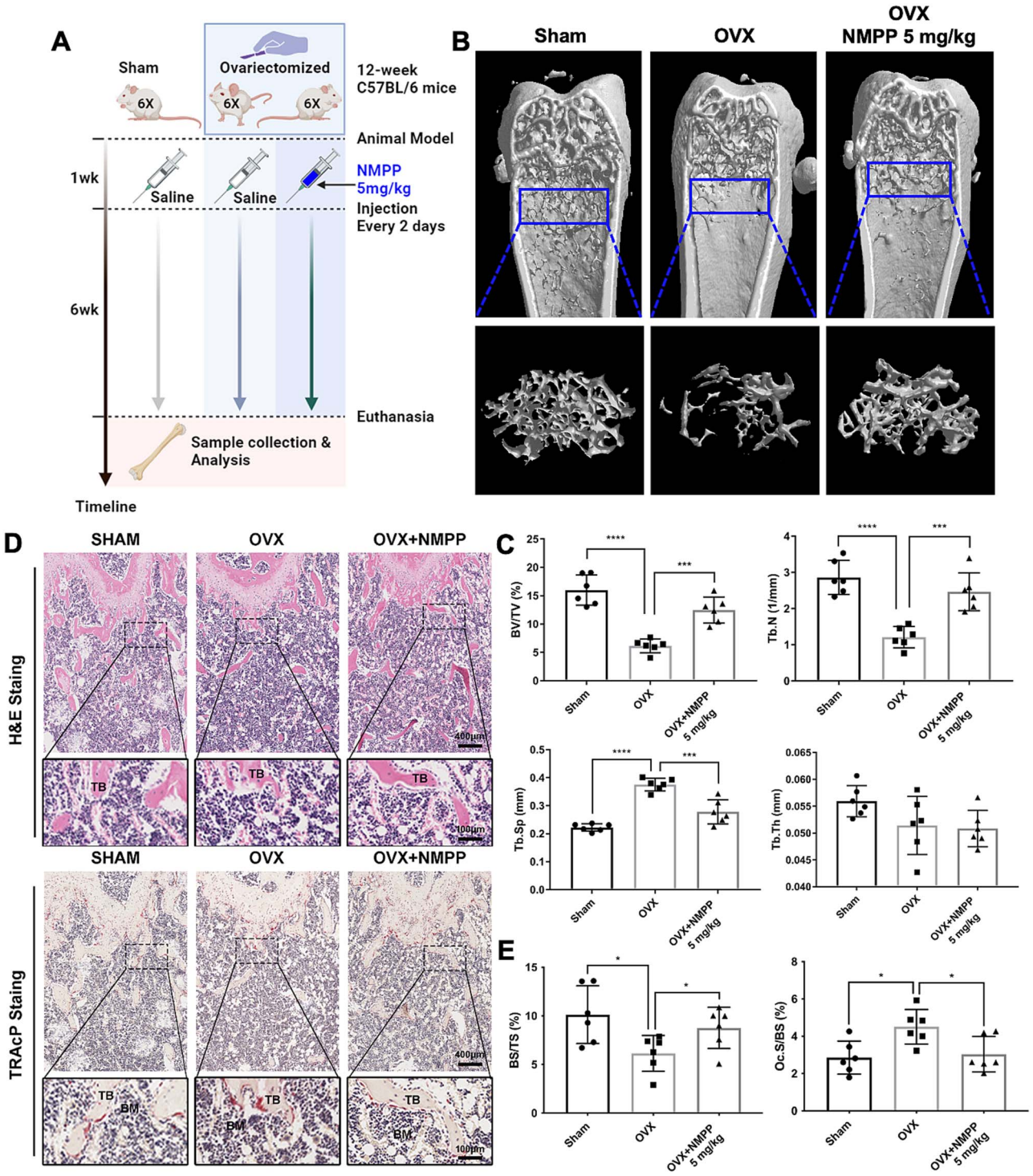

Figure 7. In vivo treatment of NMPP alleviated OVX-induced bone loss. (A) The schematic diagram of in vivo experimental design to study the protective effect of NMPP on OVX mice. (B) Representative images of micro-CT, which show that NMPP evidently rescued the excessive bone loss caused by ovariectomy. (C) The quantitative analyses of micro-CT results, including BV/TV, Tb.N, Tb.Sp and Tb.Th. $N = 6$. (D) Representative images of HE and TRAcP staining for decalcified bone tissues collected from sham mice, OVX mice treated with or without 5 mg/kg NMPP, respectively. (E) Quantification of histological measurements, including BS/TS (%) and Oc.S/BS (%). All data are presented as mean ± SD. $^{*}p < .05$, $^{**}p < .01$, $^{***}p < .001$ and $^{****}p < .0001$ compared to OVX group unless indicated otherwise. Abbreviations: BM: Bone marrow; BS/TS, bone surface/total surface; BV/TV, bone volume/tissue volume; HE, hematoxylin and eosin; Oc.S/BS, osteoclast surface/bone surface; TB, trabecular bone; Tb.N, trabecular number; Tb.Sp, trabecular separation; Tb.Th, trabecular thickness; TRAcP, tartrate-resistant acid phosphatase.

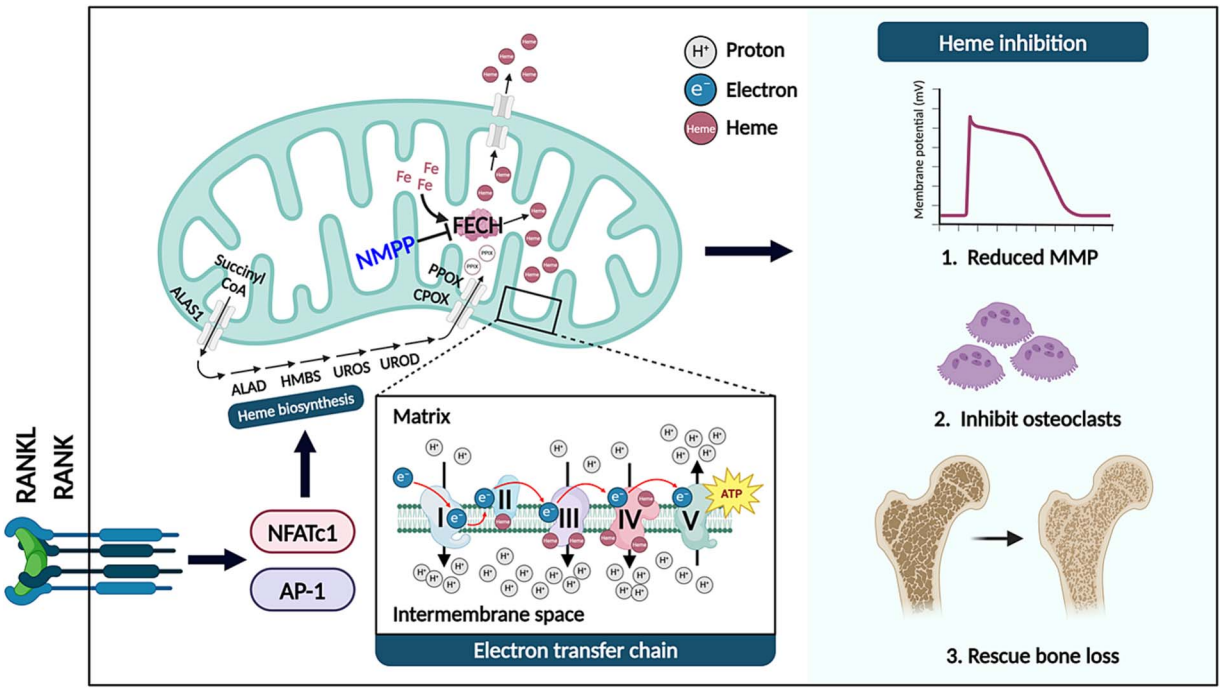

Figure 8. Graphical abstract illustrates the main findings of this study. RANKL-RANK signaling enhanced heme metabolism partially through transcription factors NFATc1 and AP-1, in which the elevated heme activity was coupled with mitochondrial biogenesis to facilitate OXPHOS, producing ATPs that boosted OC formation. Inhibition of heme biosynthesis by NMPP exhibited a dose-dependent inhibitory effect in MMP and osteoclastogenesis, reversing the excessive bone loss caused by ovariectomy. This study proposes a novel therapeutic target for osteoporosis.

mitochondria to synergistically fuel osteoclastogenesis. We first knocked down FECH in freshly isolated BMMs using shRNA and found that disruption of the Fech gene significantly hampered the formation of RANKL-induced TRAcP+ OCs, which is solidly evidenced by the reduced expression levels of osteoclastic markers at mRNA and protein levels, suggesting the essentialness of heme biosynthesis in OC biology. Meanwhile, we studied Fech as a novel therapeutic target via heme selective inhibitors, NMPP and Griseofulvin. Structural analyses of both Fech-NMPP and Fech-Griseofulvin complexes, whether derived from humans or mice, reveal that these 2 compounds interact with highly conserved residues. These residues are also engaged by the Fech-PPIX complex. Such interactions compromise the function of Fech, which is to convert PPIX into heme. Next, we examined the effect of heme in OC differentiation using NMPP. We observed synergetic increases in mitochondrial markers and MMP following RANKL treatment. The increased MMP was dose-dependently blocked by NMPP, manifesting that heme is indispensable to OXPHOS activity.[29,30,37,38] We further showed that NMPP reduced the heme level and suppressed OC formation in a dose-dependent manner independent of PPIX accumulation. The inhibitory effect of NMPP is accompanied with decreased activity of osteoclastic master transcription factors AP-1 and NF-kB. Surprisingly, we found that a single-dose treatment of NMPP on day 3 during RANKL-induced OC differentiation presented a stronger inhibitory effect than those of day 1 and day 5 only. This phenomenon is possibly related to the nature of mitochondrial biogenesis and heme metabolism in OCs. As shown by Zeng et al., the copy number of 5 mitochondrial complexes was significantly upregulated on day 3 upon RANKL stimulation.[32] Consistently, shown by our scRNA-seq analysis, both mitochondrial markers and the Fech gene were expressed at maximum during the transition from preosteoclasts to mature OCs, which usually takes place after 3-day stimulation of RANKL (Day 3). Thus, it is reasonable to observe the maximum effect of NMPP when administrated at this critical stage. Single-dose treatment with heme inhibitors offers an attractive and potent therapeutic strategy against osteolytic bone diseases. The in vivo investigation of NMPP produced results consistent with the in vitro study, in which the compromised bone volume and microarchitecture induced by estrogen deficiency were evidently reversed by NMPP treatment without noticeable side effects or other safety concerns. Declining trends of OC surface in OVX mice treated with NMPP provide a mechanistic insight that consolidates the previous observations. These results combine to manifest the clinical potential of Fech inhibitors in the treatment of osteoporosis.

Despite toxicity concerns over inhibiting mitochondrial activity, no detrimental effects on cell viability or proliferation were observed with NMPP's effective doses. This is consistent with Basavarajappa et al.'s results, which could be related to OCs' unique sensitivity to energy changes, presenting a therapeutic window similar to EGFR inhibitors.[39,40] While heme inhibition poses safety risks, daily 750 mg doses of the FDA-approved heme inhibitor Griseofulvin show no anemia risk over 6 months, suggesting its potential for osteoporosis treatment.

In summary, human and murine OC differentiation involves the coupling of mitochondrial biogenesis and heme metabolism. Heme synthesis is essential for energy production and osteoclastogenesis, in which either genetically silencing FECH or inhibition of heme synthesis with NMPP significantly hindered RANKL-induced OC formation. In addition, NMPP effectively reversed the osteoporotic phenotype in

mice without causing side effects. This may represent a novel druggable target against osteoporosis.

Author contributions

Heng Qiu (Data curation, Formal analysis, Investigation, Methodology, Validation, Visualization, Writing—original draft, Writing—review & editing), Haiming Jin (Data curation, Formal analysis, Investigation, Resources, Writing—review & editing), Jiansen Miao (Data curation, Formal analysis, Investigation, Validation, Writing—review & editing), Hui Li (Investigation), Junchun Chen (Investigation), Xiaohong Yang (Data curation, Resources, Visualization, Writing—review & editing), Xiaojun Chen (Methodology, Resources, Software, Visualization), Benjamin H. Mullin (Methodology, Resources, Software, Visualization), Kai Chen (Investigation, Methodology, Resources, Writing—review & editing), Ronghe Gu (Methodology, Resources), An Qin (Methodology, Resources, Writing—review & editing), Scott Wilson (Methodology, Resources), and Jiake Xu (Conceptualization, Funding acquisition, Project administration, Resources, Supervision, Writing—review & editing). Heng Qiu, Haiming Jin, and Jiansen Miao are equal contributors. We have added Hui Li and Junchun Chen as they contributed largely to the revision data and processes.

Heng Qiu, Haiming Jin and Jiansen Miao contributed equally to this work.

Supplementary material

Supplementary material is available at *Journal of Bone and Mineral Research* online.

Funding

This study was supported in part by the National Natural Science Foundation of China (Grant No. 82350710800, 82374470, 82202757), National Key R&D Program of China (2024YFA0919200), Shenzhen Science and Technology Program (KCXFZ20240903094059020) and Shenzhen Medical Research Fund B2302005, and NHMRC, APP1163933.

Conflicts of interest

None declared.

Data availability

This study includes no data deposited in external repositories. All data reported in this paper will be shared by the lead contact upon request.

References

1. Compston JE, McClung MR, Leslie WD. Osteoporosis. *Lancet*. 2019;393(10169):364–376. https://doi.org/10.1016/S0140-6736(18)32112-3
2. Lorentzon M. Treating osteoporosis to prevent fractures: current concepts and future developments. *J Intern Med*. 2019;285(4):381–394. https://doi.org/10.1111/joim.12873
3. Lemma S, Sboarina M, Porporato PE, et al. Energy metabolism in osteoclast formation and activity. *Int J Biochem Cell Biol*. 2016;79(2016):168–180. https://doi.org/10.1016/j.biocel.2016.08.034
4. Da W, Tao L, Zhu Y. The role of osteoclast energy metabolism in the occurrence and development of osteoporosis. *Front Endocrinol (Lausanne)*. 2021;12(2021):675385. https://doi.org/10.3389/fendo.2021.675385
5. Kim JM, Jeong D, Kang HK, Jung SY, Kang SS, Min BM. Osteoclast precursors display dynamic metabolic shifts toward accelerated glucose metabolism at an early stage of RANKL-stimulated osteoclast differentiation. *Cell Physiol Biochem*. 2007;20(6):935–946. https://doi.org/10.1159/000110454
6. Rashid S, Wilson SG, Zhu K, Walsh JP, Xu J, Mullin BH. Identification of differentially expressed genes and molecular pathways involved in osteoclastogenesis using RNA-seq. *Genes (Basel)*. 2023;14(4). https://doi.org/10.3390/genes14040916
7. Morris JA, Kemp JP, Youlten SE, et al. An atlas of genetic influences on osteoporosis in humans and mice. *Nat Genet*. 2019;51(2):258–266. https://doi.org/10.1038/s41588-018-0302-x
8. Mishra A, Macgregor S. VEGAS2: software for more flexible gene-based testing. *Twin Res Hum Genet*. 2015;18(1):86–91. https://doi.org/10.1017/thg.2014.79
9. Mullin BH, Tickner J, Zhu K, et al. Characterisation of genetic regulatory effects for osteoporosis risk variants in human osteoclasts. *Genome Biol*. 2020;21(1):80. https://doi.org/10.1186/s13059-020-01997-2
10. Mullin BH, Zhu K, Xu J, et al. Expression quantitative trait locus study of bone mineral density GWAS variants in human osteoclasts. *J Bone Miner Res*. 2018;33(6):1044–1051. https://doi.org/10.1002/jbmr.3412
11. Tsukasaki M, Huynh NC, Okamoto K, et al. Stepwise cell fate decision pathways during osteoclastogenesis at single-cell resolution. *Nat Metab*. 2020;2(12):1382–1390. https://doi.org/10.1038/s42255-020-00318-y
12. Ng AY, Tu C, Shen S, et al. Comparative characterization of osteoclasts derived from murine bone marrow macrophages and RAW 264.7 cells using quantitative proteomics. *JBMR Plus*. 2018;2(6):328–340. https://doi.org/10.1002/jbm4.10058
13. Chen K, Qiu P, Yuan Y, et al. Pseurotin a inhibits Osteoclastogenesis and prevents ovariectomized-induced bone loss by suppressing reactive oxygen species. *Theranostics*. 2019;9(6):1634–1650. https://doi.org/10.7150/thno.30206
14. Qiu H, Hosking C, Rothzerg E, et al. ADR3, a next generation i-body to human RANKL, inhibits osteoclast formation and bone resorption. *J Biol Chem*. 2023;299(2):102889. https://doi.org/10.1016/j.jbc.2023.102889
15. Chiabrando D, Marro S, Mercurio S, et al. The mitochondrial heme exporter FLVCR1b mediates erythroid differentiation. *J Clin Invest*. 2012;122(12):4569–4579. https://doi.org/10.1172/JCI62422
16. Qiu H, Qin A, Cheng T, et al. A missense mutation sheds light on a novel structure-function relationship of RANKL. *J Cell Physiol*. 2021;236(4):2800–2816. https://doi.org/10.1002/jcp.30045
17. Audronė V, Kalvelytė AI, Krestnikova N, Stulpinas A. Chapter 4: – adult stem cells and anticancer therapy. In: Fishbein JMHJC, ed. *Advances in Molecular Toxicology*. Elsevier; 2017:123–202 https://doi.org/10.1016/B978-0-12-812522-9.00004-X.
18. Huber DM, Bendixen AC, Pathrose P, et al. Androgens suppress osteoclast formation induced by RANKL and macrophage-colony stimulating factor. *Endocrinology*. 2001;142(9):3800–3808. https://doi.org/10.1210/endo.142.9.8402
19. Luegmayr E, Glantschnig H, Wesolowski GA, et al. Osteoclast formation, survival and morphology are highly dependent on exogenous cholesterol/lipoproteins. *Cell Death Differ*. 2004;11(S1):S108–S118. https://doi.org/10.1038/sj.cdd.4401399
20. Glantschnig H, Fisher JE, Wesolowski G, Rodan GA, Reszka AA. M-CSF, TNFalpha and RANK ligand promote osteoclast survival by signaling through mTOR/S6 kinase. *Cell Death Differ*. 2003;10(10):1165–1177. https://doi.org/10.1038/sj.cdd.4401285
21. Cornish J, MacGibbon A, Lin JM, et al. Modulation of osteoclastogenesis by fatty acids. *Endocrinology*. 2008;149(11):5688–5695. https://doi.org/10.1210/en.2008-0111
22. Taubmann J, Krishnacoumar B, Bohm C, et al. Metabolic reprogramming of osteoclasts represents a therapeutic target during the treatment of osteoporosis. *Sci Rep*. 2020;10(1):21020. https://doi.org/10.1038/s41598-020-77892-4
23. Nilsson R, Schultz IJ, Pierce EL, et al. Discovery of genes essential for heme biosynthesis through large-scale gene expression

analysis. *Cell Metab*. 2009;10(2):119–130. https://doi.org/10.1016/j.cmet.2009.06.012
24. Krager KJW, Wang L, Fujiwara T, et al. The murine osteoclasts lacking transferrin receptor 1 have altered mitochondrial metabolism, cytoskeletal organization and increased trabecular bone mass. *Free Radic Biol Med*. 2017;112(Suppl 1):168–169 https://www.sciencedirect.com/science/article/abs/pii/S0891584917310468
25. Lehenkari P, Hentunen TA, Laitala-Leinonen T, Tuukkanen J, Vaananen HK. Carbonic anhydrase II plays a major role in osteoclast differentiation and bone resorption by effecting the steady state intracellular pH and Ca2+. *Exp Cell Res*. 1998;242(1):128–137. https://doi.org/10.1006/excr.1998.4071
26. Wu C, Jin X, Tsueng G, Afrasiabi C, Su AI. BioGPS: building your own mash-up of gene annotations and expression profiles. *Nucleic Acids Res*. 2016;44(D1):D313–D316. https://doi.org/10.1093/nar/gkv1104
27. Rouillard AD, Gundersen GW, Fernandez NF, et al. The harmonizome: a collection of processed datasets gathered to serve and mine knowledge about genes and proteins. *Database (Oxford)*. 2016;2016:1–16. https://doi.org/10.1093/database/baw100
28. Yien YY, Robledo RF, Schultz IJ, et al. TMEM14C is required for erythroid mitochondrial heme metabolism. *J Clin Invest*. 2014;124(10):4294–4304. https://doi.org/10.1172/JCI76979
29. Shetty T, Sishtla K, Park B, Repass MJ, Corson TW. Heme synthesis inhibition blocks angiogenesis via mitochondrial dysfunction. *iScience*. 2020;23(8):101391. https://doi.org/10.1016/j.isci.2020.101391
30. Chandana M, Anand A, Ghosh S, et al. Malaria parasite heme biosynthesis promotes and griseofulvin protects against cerebral malaria in mice. *Nat Commun*. 2022;13(1):4028. https://doi.org/10.1038/s41467-022-31431-z
31. Shi Z, Ferreira GC. Modulation of inhibition of ferrochelatase by N-methylprotoporphyrin. *Biochem J*. 2006;399(1):21–28. https://doi.org/10.1042/BJ20060753
32. Zeng R, Faccio R, Novack DV. Alternative NF-kappaB regulates RANKL-induced osteoclast differentiation and mitochondrial biogenesis via independent mechanisms. *J Bone Miner Res*. 2015;30(12):2287–2299. https://doi.org/10.1002/jbmr.2584
33. Stephens S. *Novel Osteoclast Signalling* PhD Doctorate. Griffith University; 2010.
34. Kim HJ, Khalimonchuk O, Smith PM, Winge DR. Structure, function, and assembly of heme centers in mitochondrial respiratory complexes. *Biochim Biophys Acta*. 2012;1823(9):1604–1616. https://doi.org/10.1016/j.bbamcr.2012.04.008
35. Atamna H, Killilea DW, Killilea AN, Ames BN. Heme deficiency may be a factor in the mitochondrial and neuronal decay of aging. *Proc Natl Acad Sci USA*. 2002;99(23):14807–14812. https://doi.org/10.1073/pnas.192585799
36. Alam MM, Lal S, FitzGerald KE, Zhang L. A holistic view of cancer bioenergetics: mitochondrial function and respiration play fundamental roles in the development and progression of diverse tumors. *Clin Transl Med*. 2016;5(1):3. https://doi.org/10.1186/s40169-016-0082-9
37. Lamsa V, Levonen AL, Sormunen R, Yamamoto M, Hakkola J. Heme and heme biosynthesis intermediates induce heme oxygenase-1 and cytochrome P450 2A5, enzymes with putative sequential roles in heme and bilirubin metabolism: different requirement for transcription factor nuclear factor erythroid-derived 2-like 2. *Toxicol Sci*. 2012;130(1):132–144. https://doi.org/10.1093/toxsci/kfs237
38. Atamna H, Brahmbhatt M, Atamna W, Shanower GA, Dhahbi JM. ApoHRP-based assay to measure intracellular regulatory heme. *Metallomics*. 2015;7(2):309–321. https://doi.org/10.1039/c4mt00246f
39. Basavarajappa HD, Sulaiman RS, Qi X, et al. Ferrochelatase is a therapeutic target for ocular neovascularization. *EMBO Mol Med*. 2017;9(6):786–801. https://doi.org/10.15252/emmm.201606561
40. Ranson M. Epidermal growth factor receptor tyrosine kinase inhibitors. *Br J Cancer*. 2004;90(12):2250–2255. https://doi.org/10.1038/sj.bjc.6601873

Journal of Bone and Mineral Research, 2025, 40, 639–655
https://doi.org/10.1093/jbmr/zjaf040
Research Article